A comparative study on microstructure and properties of traditional laser cladding and high-speed laser cladding of Ni45 alloy coatings

Wuyan Yuan[1], Ruifeng Li[1,*], Zhaohui Chen[1], Jiayang Gu[2], Yingtao Tian[3]

1. School of Materials Science and Engineering, Jiangsu University of Science and Technology, Zhenjiang, Jiangsu, 212003, P. R. China

2. Marine Equipment and Technology Institute, Jiangsu University of Science and Technology, Zhenjiang, Jiangsu, 212003, P. R. China

3. Department of Engineering, Lancaster University, Bailrigg, Lancaster LA1 4YW, UK

*Correspondence: Dr Ruifeng Li (li_ruifeng@just.edu.cn)

Abstract:

High-speed laser cladding technology can significantly improve the efficiency of coating preparation and effectively widen the application range of laser cladding. In this study, the Ni45 powders were deposited on steel substrate by traditional low speed laser cladding and high-speed laser cladding process, respectively. The cladding efficiency, surface forming, cross-sectional microstructure, microhardness, wear and corrosion resistance properties of the traditional and high-speed laser cladded Ni45 alloy coatings were compared. It can be seen that the thickness of the high-speed laser cladding coating was much thinner than that of the traditional laser cladding coating. Compared with traditional laser cladding, high-speed laser cladding could achieve a cladding speed of 76.86 m/min and a cladding efficiency of 156.79 cm^2/min. The microstructure of the two kinds of coatings shows the same growth law, but the microstructure in high-speed laser cladding was smaller and denser, and the columnar crystal interval was narrower, only about 6 μm. It is found that the cooling rate of the traditional laser cladding coating was smaller than that of the high-speed laser cladding, and as the cladding speed increased, the cooling rate became higher and higher. The cross-section microhardness of the traditional laser cladding coating was relatively uniform of 337 $HV_{0.2}$, while the

microhardness of high-speed laser cladding surface increased to about 543 $HV_{0.2}$. In addition, the wear and corrosion resistance of high-speed laser cladded coatings were better than that of traditional laser cladded coatings. As the cladding speed increased, the wear and corrosion resistance of the cladded coatings became better.

1   Introduction

The surface of the workpiece or the area near the surface may be damaged by wear, corrosion and fatigue during service. The sustained damage will cause severe damage to the surface of the material until it can no longer be used [1]. Therefore, it is crucial to study the new coating material to protect the surface of the material. When using wear-resistant and corrosion-resistant coatings, the material composition of the workpiece at this time will no longer be restricted by the required performance characteristics of mechanical, friction, chemical, or mechanical surface layer, as well as thermoelastic aspects, so that resource-saving workpieces can be used [2]. Up to now, hard chrome coating (HCP) is mainly used for the wear and corrosion protective layer of hydraulic and pneumatic piston rods and cylinders, valves, pump shafts and various rotors in the aviation, automotive, oil and gas industries [3]. Hard chromium plating is a traditional surface electroplating technology, which is a thick chromium coating on various substrate surfaces. Its thickness is generally more than 20μm. The characteristics of chromium can be used to improve the hardness, wear resistance, mild corrosion resistance and other properties of the parts. High hardness chromium plating (up to 1200 HV) provides higher wear resistance and increases roll life. In addition, the chromium coating helps prevent the adhesive transfer of the viscous alloy. According to the

relevant literature, chromium plating can produce up to 20% difference in the value of reflective bands, which can be used to quantify iron powder [4]. Nevertheless, the production and use of HCP are increasingly restricted by countries, particularly developed countries, because of the presence of toxic and carcinogenic hexavalent chromium (Cr^{+6}) in HCP. The United States, the Netherlands, and the United Kingdom reduce Cr^{+6} PEL to $5\mu g/m^3$, $1.5\mu g/m^3$, and $0.5\mu g/m^3$, respectively. In addition to specifying the Cr^{+6} content in the working ambient air, EPA also strictly specifies the daily maximum limit and monthly average limit of the total amount of chromium in the waste liquid produced by chromium plating [5, 6]. The coating technologies considered to replace HCP are thermal spraying technology, high-speed oxygen fuel thermal spraying (HVOF), and laser cladding (LD). For HVOF, it can reduce the thermal diffusivity and improve the high-temperature corrosion resistance, which has been effectively applied in many industries [7]. But it also has some limitations, such as the low bond strength between the spray coating and the substrate, the substrate surface treatment must be reasonable and so on.

The advanced laser cladding technology can make use of its metallurgical combination and low dilution rate to prepare high-quality, void-free, and crack-free coatings in a variety of materials [8]. However, the use of laser cladding coatings in the production of wear and corrosion protective coatings is still limited because the thickness of traditional laser cladding coatings (>500 m) is generally too large for wear and corrosion protection. Moreover, the surface preparation rate of traditional laser cladding is within the range of 10-50 cm^2/min, which is too inefficient for the coating of large components [9]. Fraunhofer [10] Laser Technology Research Institute in Aachen, Germany, developed an ultra-high-speed laser cladding technology, which enabled the surface rate of laser cladding to reach 500 cm^2/min

and the speed of cladding line to reach 200 m/min, significantly improving the preparation efficiency of laser cladding coating. Furthermore, through the high-speed laser cladding process, a thinner, non-porous, crack-free wear-resistant and corrosion-resistant protective layer with a thickness of about 10-250 μm can be produced.

Damian et al. [11] prepared a new nickel-based coating through the traditional laser cladding process, which can further inhibit the corrosion oxidation caused by air and improve the corrosion resistance of 13CrMo4-5 steel. Li et al. [12] coated the TI-CuNiCoAlTaY composite coating on TC4 alloy by traditional laser cladding and found that the high oxidation resistance of the coating was sufficient to improve the flame retardant property of the material after the laser point-melting test at 800℃. Soboleva et al. [13] effectively improved the residual compressive stress of the substrate by preparing NiCrBSi coating and conducting deformation treatment. Xu et al. [14] prepared CuAlNiCrFe high-entropy alloy coating by high-speed laser cladding test, which controlled the phase 3 between matrix and binding layer within a very small range and improved the collective antioxidant capacity.

In addition, compared with traditional surface modification techniques such as spray welding and surfacing welding, the nickel-based coating used in laser cladding experiments has good toughness, heat resistance, oxidation resistance, impact resistance, and corrosion resistance and is widely used in various aspects [15, 16]. Ni45 self-melting alloy is a widely used cladding material with moderate strength and toughness, excellent physicochemical compatibility with 45 steel substrate, easy to obtain high density, good metallurgical combination with the substrate and crack-free alloy coating [17, 18].

At present, there have been preliminary studies on high-speed laser cladding Ni-based coating at home and abroad, and a large number of studies have been conducted on traditional

laser cladding Ni-based coating at home and abroad. However, the differences between the performance of high-speed laser cladding coating and traditional cladding Ni-based coating and the reasons for the differences have not been reported in detail. Therefore, this paper focuses on the comparison and analysis of the differences between traditional and high-speed laser cladding Ni-based coatings in terms of structure and properties.

2 Materials and methods

2.1 Experimental materials

2.1.1 Alloy powder

Due to the faster cladding speed in high-speed laser cladding, the amount of powder melted per unit time is much larger than that of traditional laser cladding, which has higher requirements for powder particle size and powder feeding speed. Therefore, the alloy powder with smaller particle size is used in high-speed laser cladding, which not only improves the efficiency of powder feeding but also improves the melting efficiency of powder. The particle size of two Ni45 alloy powders used in this experiment for high-speed laser cladding and traditional laser cladding were compared and analyzed. Two kinds of Ni45 alloy powders were bought from Changsha Tianjiu Metal Materials Co. LTD. The mesh number of the traditional Ni45 alloy powder is -150~+320, and the mesh number of high-speed laser cladding Ni45 alloy powder is -320. The scanning electron microscope images are shown in Fig. 1. As shown in the Fig.1 , the two powders are spherical or ellipsoidal except for their different diameters and particle sizes, which ensures the smoothness and continuity of powder feeding during the experiment and improves the melting efficiency of the powder. The chemical composition of Ni45 is shown in Table 1.

Table 1 Chemical composition of Ni45 nickel-based alloy powder

| C	Cr	Si	Mn	Fe	B	Ni
0.45	12.00	4.00	0.10	10.00	2.40	Bal
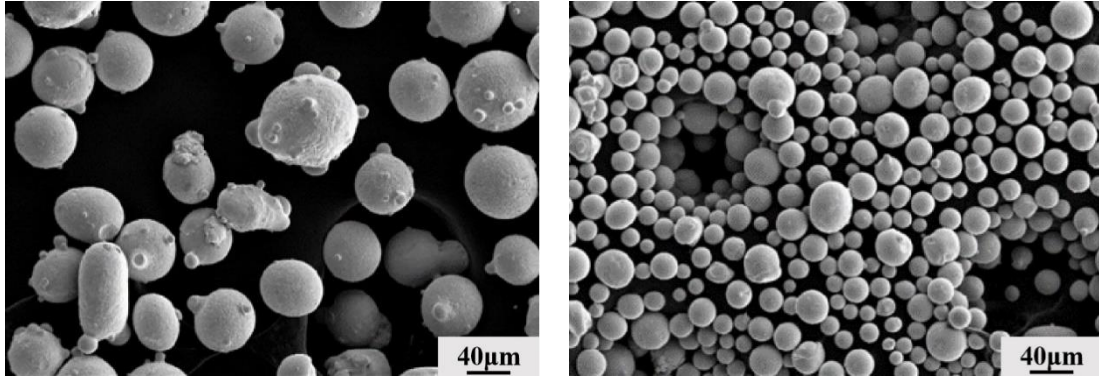
(a) Traditional laser cladding   (b) High-speed laser cladding

Fig. 1 SEM morphology of two kinds of Ni45 alloy powders

The particle analysis software called Nano measure was used to measure the powder diameter in Fig. 1, and the measured data were mapped as shown in Fig. 2. The diameters of the powder used in traditional laser cladding were mainly concentrated between 55 and 75 μm, and the average size was 66.9 μm. The diameters of the powder used in high-speed laser cladding were primarily concentrated between 15 and 30 μm, and its average size was 23.61 μm. It can be seen that the particle size of the powder used in high-speed laser cladding is much smaller than that used in traditional laser cladding.
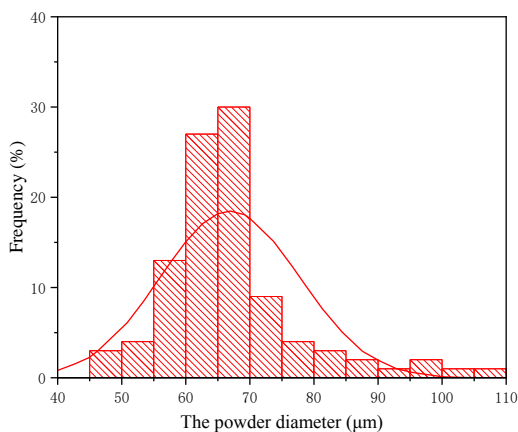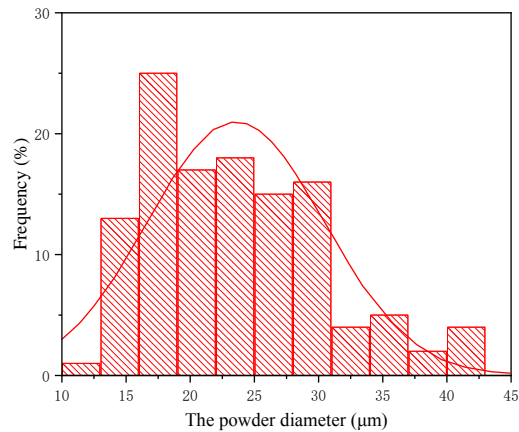
(a) Traditional laser cladding   (b) High-speed laser cladding

Fig. 2 The diameter distribution of two Ni45 alloy powders

2.1.2 Substrate material

The substrate material used in the paper is 45 medium carbon steel (AISI 1045), which is a high-quality carbon structural steel with a hardness value of about 200 HV. The chemical composition is shown in Table 2. The substrate material's Rm(tensile strength) $\geq$ 600 MPa, and its $Rp_{0.2}$(yield strength)$\geq$ 355 MPa. Due to its excellent properties, high strength, good plasticity and toughness, as well as abundant resources, it has been widely used in many industrial fields [19]. In the experiment, a 45 steel cylinder with a diameter of 40 mm and a length of 120 mm was selected and cleaned with acetone alcohol before cladding.

Table 2 Chemical composition of 45 steel

Element	C	Si	Mn	Cr	Ni	Cu	Fe
Content (%)	0.42~0.50	0.17~0.37	0.50~0.80	0.25	0.30	0.25	margin

2.2 High-speed laser cladding system

Fig. 3 shows the high-speed laser cladding experimental platform, which includes three parts: high-speed lathe, laser and powder feeding system and 45 steel shaft. Among them, the powder feeding system and laser are integrated on the laser head of the front end of the ABB robot, and the preset moving trajectory is set by programming control. During the cladding process, the high-speed machine tool drove the pretreated 45 steel shaft to rotate, and the laser head was driven by the robot to move along the direction of the steel shaft above the steel shaft. The laser melted the powder and a small amount of substrate to form a molten pool on the surface of the steel shaft. After the laser was removed, the self-cooling solidified to form a

coating. Finally, a uniform nickel-based coating cladding the entire surface of the steel shaft was obtained. Unlike traditional laser cladding, the laser focus and powder focus in high-speed laser cladding were located above the surface of the steel shaft, and the powder had been heated and partially melted before contacting the surface of the steel shaft.
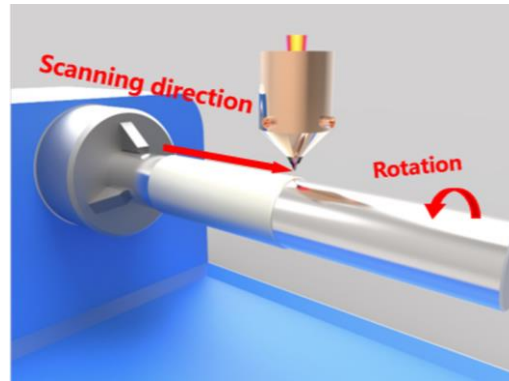

Fig. 3 High-speed laser cladding experimental platform

2.3 Experimental characterization

2.3.1 Microstructure and phase constitution characterization

The coating and a small amount of substrate were cut off by wire cutting, cleaned with acetone after polishing, and then ultrasonically cleaned with alcohol. The phase composition of the coating was analyzed by XRD-6000X ray diffractometer, using a voltage of 40 kV, a Cu target, a scanning range of 20~90°, a scanning speed of 4°/min, and a step size of 0.02°. Ultrasonic cleaning was carried out on the cut samples with acetone and alcohol. After water milling and polishing, the samples were wiped and corroded by aqua regia for several times until the clear grains could be observed under the optical microscope. The micro-morphology of the coating was analyzed by Merlin CoMPact scanning electron microscope.

2.3.2 Mechanical properties characterization

The HXS-1000AC touch semi-automatic microhardness tester was used to test the hardness of the cladding layer cross-section. The load was 200 g and the loading time was 10 s. Multiple measurements were averaged to reduce the experimental error. The cubic of 5mm × 5mm ×5mm was cut off on the high-speed cladding workpiece. After connecting the wire on the substrate side of the sample, the cold mosaic carried out to expose the working surface of 5 mm × 5 mm on one side of the cladding layer, and then the surface was polished. A standard three-electrode system was adopted, the corrosive medium was 3.5wt % NaCl solution, the scanning speed was 1 mV/s and then the electrochemical corrosion test was carried out. The laser cladding cylindrical workpiece was cut down along the axis of the sample with a length of 15 mm, width and thickness of 5 mm, and the sandpaper was used to polish the test surface on one side of the cladding layer which the surface roughness of conventional laser cladding samples was 24.9 μm, and surface roughness of high-speed laser cladding was 13.88 μm. The linear friction and wear test of the coating in the length direction was carried out by UMT-2 friction and wear instrument. Reciprocating sliding mode was used in the experiment. the coupling parts were Si_3N_4 ceramic balls with hardness grade 8.8, load 25N, single sliding length 10mm, sliding speed 10mm/s, and sliding time of 30 min.

3 Results and discussion

3.1 Surface forming

As an advanced technology to improve the efficiency of traditional laser cladding, high-speed laser cladding not only greatly enhances the efficiency of laser cladding, but also has new forming characteristics in surface morphology, dilution rate and surface roughness. These new forming characteristics directly or indirectly affect the performance of cladding layer and the application field of the prepared coating. In order to compare the characteristics

of high-speed laser cladding with that of traditional laser cladding coating, a good composition of traditional laser cladding parameters and three groups of high-speed laser cladding parameters with different cladding speeds were selected to compare the characteristics of surface morphology, cladding efficiency, and surface roughness respectively. The test parameters are shown in Table 3.

Table 3 Traditional and high-speed laser cladding test parameters

	Number	Laser power （W）	Powder feeding voltage （V）	Cladding rate （m/min）	Lap rate （%）
Traditional laser cladding	1	2000	10	0.6	40
High-speed laser cladding	2	2000	40	37.68	40
	3	2000	40	58.02	40
	4	2000	40	76.86	40

3.1.1 Macro-appearance of the coating

The coating prepared by laser cladding is metallurgically combined with the substrate, and the bonding strength is high. Due to the large width and height of each cladding layer in the traditional laser cladding process, the existence of lap joints between welding bead caused the inevitable uneven surface of cladding layer, which required a lot of turning and further finishing treatment when applied to workpiece with higher accuracy requirements. Compared with the traditional laser cladding, the high-speed laser cladding coating had low roughness. The surface roughness was measured by laser confocal. The results showed that the line roughness and surface roughness of conventional laser cladding samples were 15.9 μm and 24.9 μm, respectively, and the roughness level was 3. In high-speed laser cladding, the surface roughness and surface roughness were 6.18 μm and 13.88 μm, respectively, and the roughness grades were 5 and 4, which were 2 and 1 levels higher than that of conventional laser cladding.

The comparison of surface roughness of conventional and high-speed laser cladding coatings is shown in Fig.4. It can be used without or greatly reducing the finishing, which improved the work efficiency and reduced the processing cost.
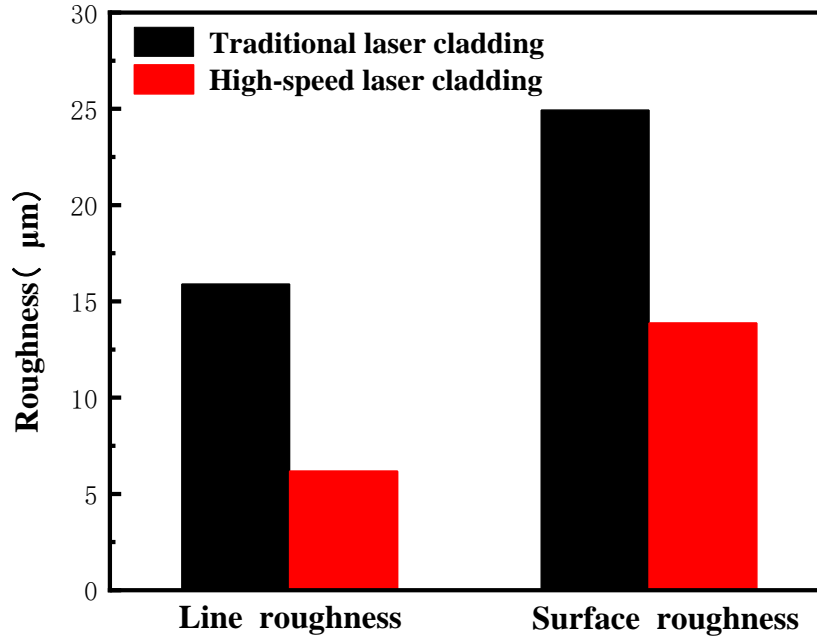

Fig.4 Comparison of surface roughness of conventional and high-speed laser cladding coatings

3.1.2 Cross-section microstructure of the coating

Fig. 5 is the cross-sectional microstructure of traditional and high-speed laser cladding coatings, of which Fig. 5(a) is a traditional laser cladding, and Fig. 5(b), (c) and (d) are high-speed laser cladding with different cladding speeds. Under each test parameter, a cladding layer with uniform thickness and good molding was obtained. It can be seen from the figure that the thickness of the traditional laser cladding coating was about 700 μm, which was much larger than the thickness of the high-speed laser cladding coating. In high-speed laser cladding, as the cladding speed increased, the thickness of the cladding layer decreased. When the cladding speed was 76.86 m/min, the thickness of the cladding layer was 53.53 μm, and it was well bonded to the substrate.

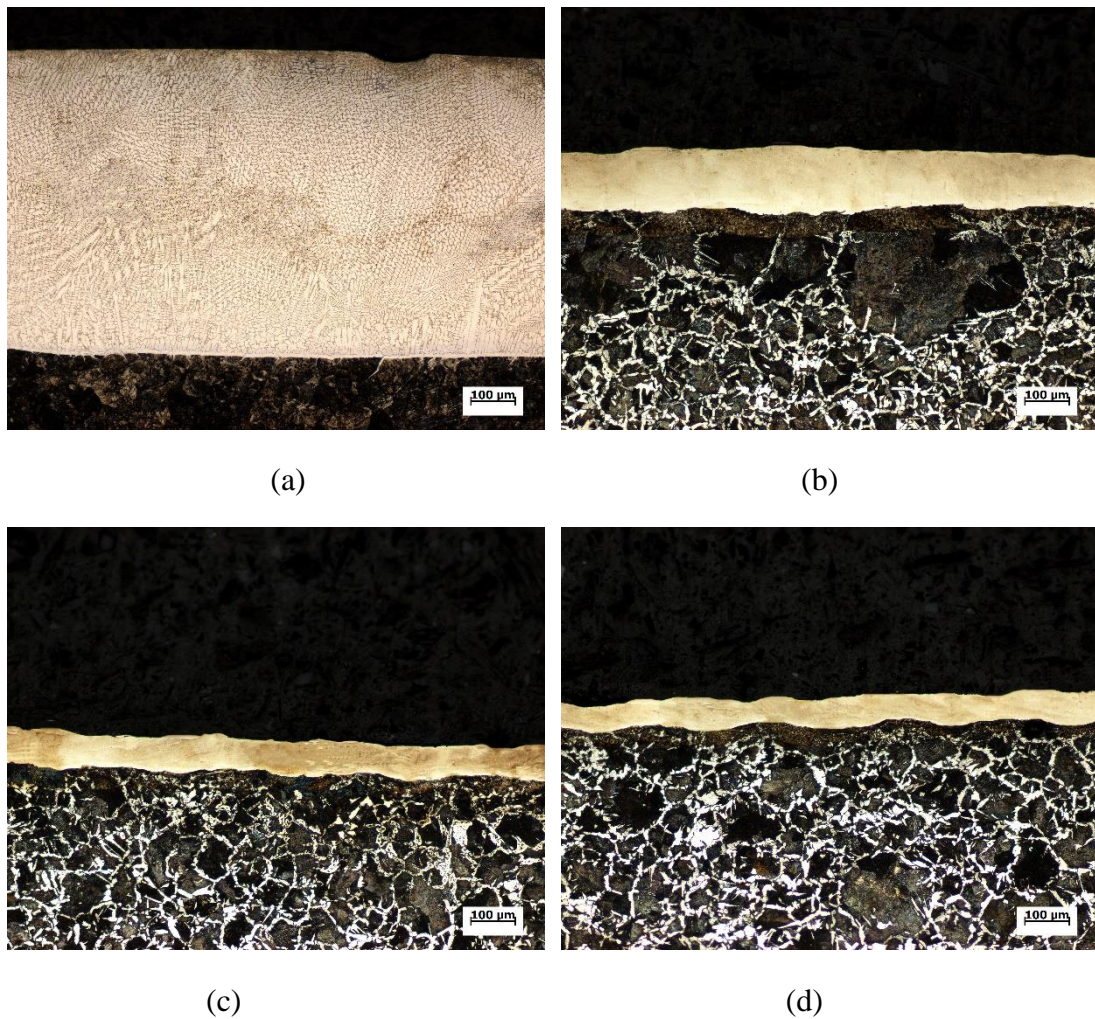(a)　　　　　　　　　　　　　　　(b)

(c)　　　　　　　　　　　　　　　(d)

Fig.5 Cross-section microstructure of the laser cladding coating at different scanning speed: (a) 0.6 m/min, (b) 37.68 m/min, (c) 58.02 m/min, (d) 76.86 m/min

3.1.3 Efficiency of laser cladding

Fig. 6 shows the comparison of the speed and efficiency of traditional laser cladding and high-speed laser cladding. The first group was the traditional laser cladding test, with the cladding speed of 0.6 m/min and the cladding efficiency of 18 cm^2/min. No. 2, 3, and 4 were all high-speed laser cladding tests, which significantly improved the cladding speed compared with traditional laser cladding. Although the width of single high-speed cladding coating was narrower than that of traditional laser cladding coating, the cladding efficiency was greatly improved under the advantage of very high cladding speed. Among them, the high cladding

speed with excellent forming was obtained in the parameter 4 test, the cladding speed was 76.86m /min, and the cladding efficiency was 156.79 cm^2 /min. Compared with traditional laser cladding, when the laser cladding speed increased from 0.6m/min to 76.86m/min, the cladding efficiency increased by 8.7 times.

Table 4 Comparison of traditional and high-speed laser cladding efficiency

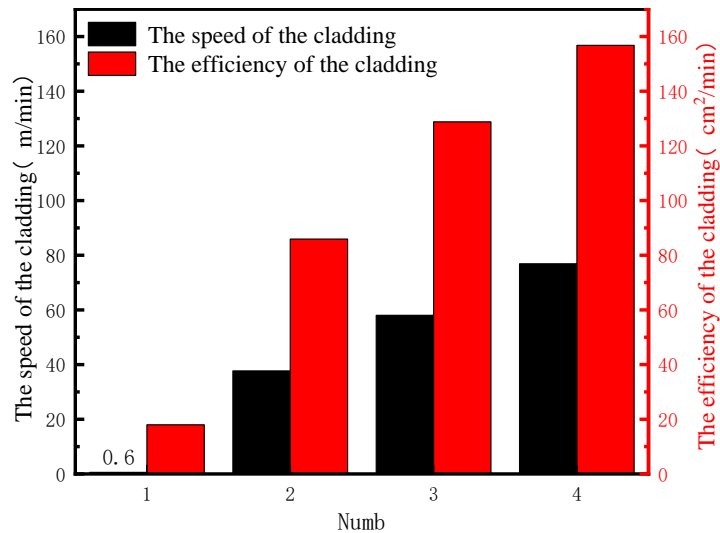| Number	1	2	3	4
Cladding speed （m/min）	0.6	37.68	58.02	76.86
Cladding efficiency （cm^2/min）	18	85.91	128.80	156.79

Fig. 6 Comparison of speed and efficiency of traditional and high-speed laser cladding
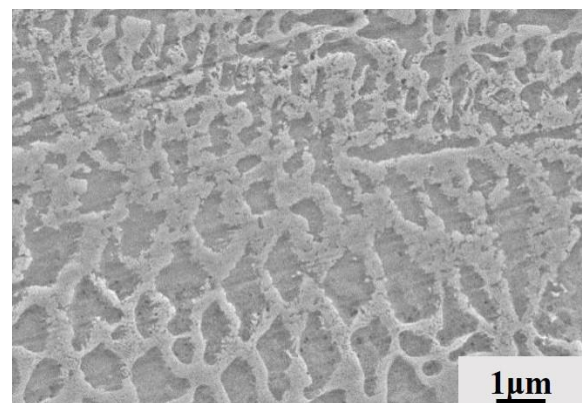
3.2 Microstructure

Fig. 7 shows the cross-sectional microstructure near the clad/substrate interface at different laser scanning speed. According to the images, the solidification structure changed from columnar crystal to dendrite structure, which could be observed in Fig. 7 (d). Moreover, the cladding layer had a higher cooling rate under the cladding speed of 76.86 m/min, and the columnar crystal formation interval was shorter. The solidification structure changed to the

equiaxial dendrite region. The structural analysis results show that no matter how the scanning speed changed, the structure changed from columnar dendritic structure to equiaxial dendritic structure from the interface to the coating surface. It can also be observed in the figure that the microstructure at the bottom of the traditional and high-speed laser cladding coating shows the same growth law. The microstructure above the metallurgical bonding zone was columnar crystal with strong orientation, and its growth direction was close to vertical to the metallurgical bonding zone. At the bottom of the cladding layer, both the traditional and high-speed laser cladding structures were columnar crystals, and the temperature gradient perpendicular to the cladding coating/interface (metallurgical bonding zone) was the largest, which was beneficial to crystallization and growth. Therefore, the growth direction of columnar crystals was perpendicular to the metallurgical bonding zone. Different from traditional laser cladding, the microstructure of high-speed laser cladding coating was finer and denser, and the columnar crystal interval was narrower, only about 6 μm, less than one-tenth of the columnar crystal interval of traditional laser cladding microstructure.

(a)   (b)

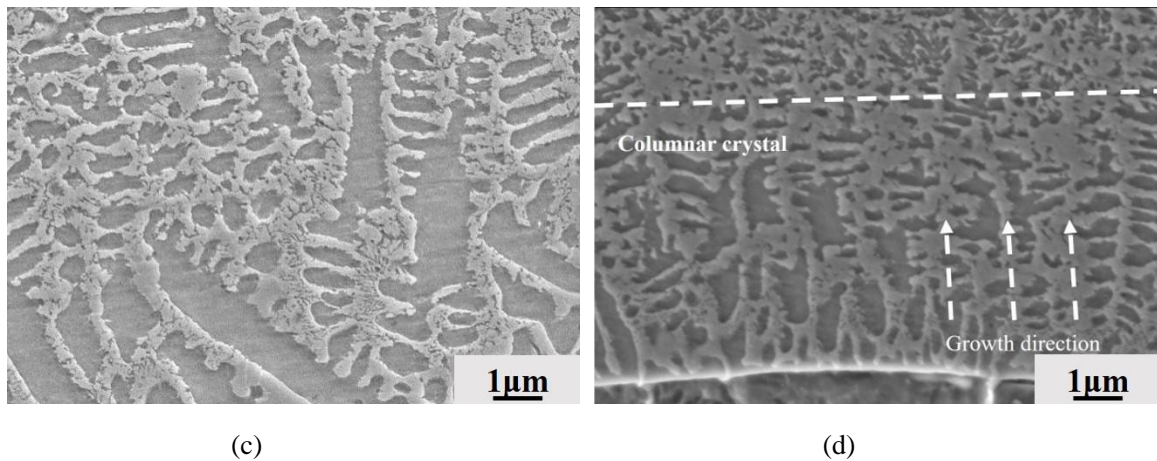(c)   (d)
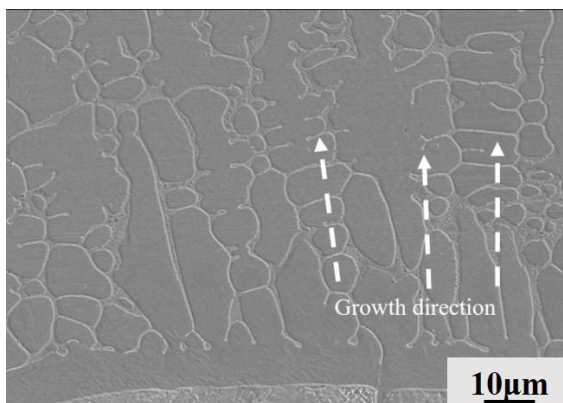
Fig. 7 Microstructure near the bottom at different laser cladding speed: (a) 0.6 m/min, (b) 37.68 m/min, (c)

58.02 m/min, (d) 76.86 m/min

The laser scanning rate significantly affects the coagulation mode. By comparing Fig. 7,

Fig. 8 and Fig. 9, it can be found that as the scan rate increased, the equiaxed crystal region

increased. Among the three samples of high-speed laser cladding, the G/R ratio decreased

under the condition of constant laser power and increased scanning rate. This is because with

the increase of laser scanning rate, the laser reaction time with the material would be reduced

and less heat would be transferred, so that the temperature gradient would be reduced. On the

other hand, R increased as the laser scanning rate increased. As a result, tissue supercooling

increased and tissue transitioned to equiaxed crystals. At a low laser scanning rate, the

structure at the top of the coating was equiaxed dendritic crystals. Considering that the R

value decreased and the temperature gradient decreased when the laser scanning rate was low,

the G/R ratio increased accordingly, and the microstructure should be columnar crystal

structure. This is not the case, and the reason for the equiaxed dendritic crystals is that some

of the dendrites in the pool, stirred by the pool, break up into new nucleating matrices on

which molten metal atoms crystallize. In addition, microstructure changes are also caused by

equiaxed grains formed by heterogeneous nucleation and microstructure supercooling in the
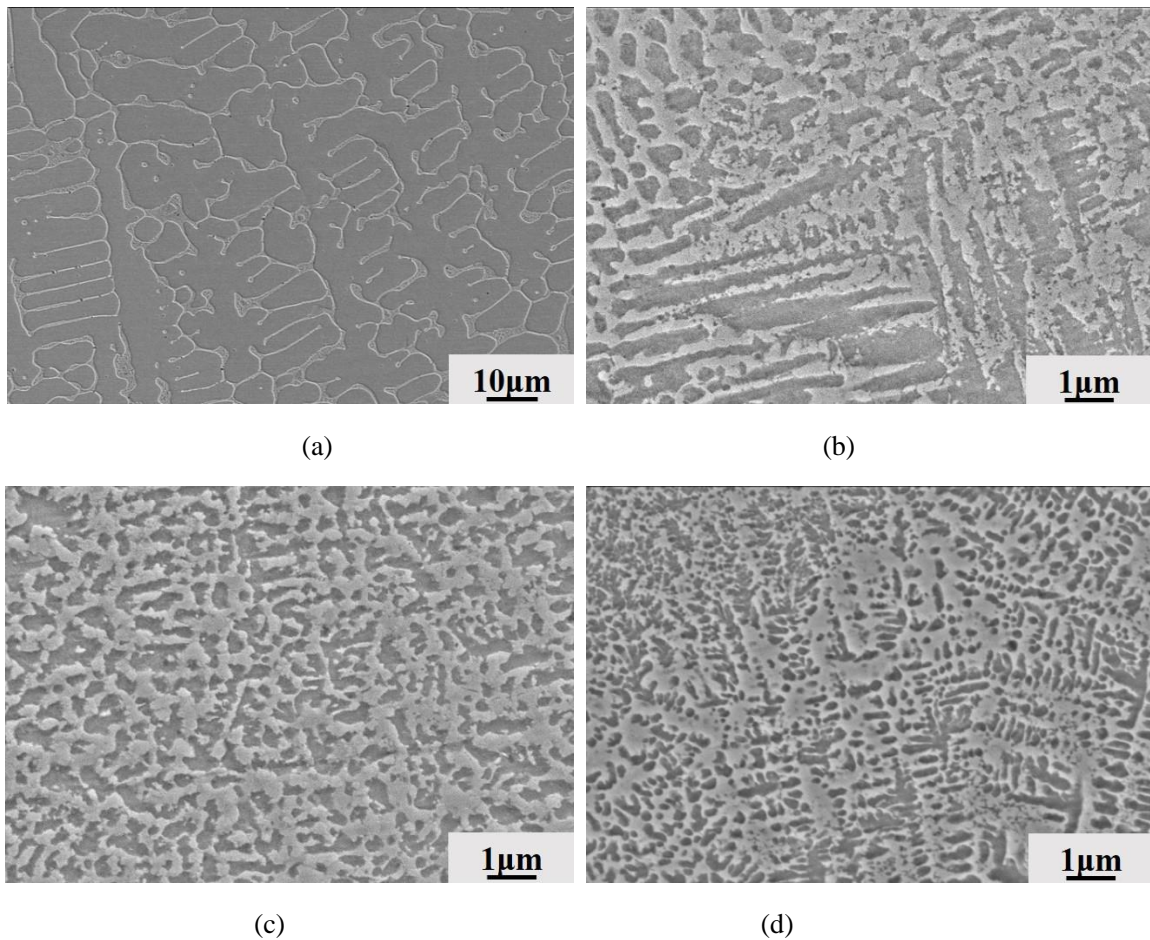
melt zone[20].

(a)   (b)

(c)   (d)

Fig. 8 Microsturcture in the middle region at different laser scanning speed: (a) 0.6 m/min, (b) 37.68 m/min,

(c) 58.02 m/min, (d) 76.86 m/min

In addition, in order to study the effect of cladding speed on the formation of nanocrystals

in high-speed laser cladding coating, Fig. 7, Fig. 8 and Fig. 9 were compared again, it is found

that only the top of the coating had nanocrystals, as shown in Fig. 9. The number and size of

nanocrystals at the top of the cladding layer were also different at different scanning speeds.

When the traditional laser cladding and scanning speed were 37.68 m/min, no nanocrystals

were found in the high-power scanning image at the top of the cladding layer, as shown in Fig.

9 (a) (b). A small number of nanocrystals were found in the high-power scanning image of the

top of the cladding layer when the scanning speed was 58.02m /min, and the size of

nanocrystals was large, about 100-200 nm, as shown in Fig. 9 (c). However, when the scanning speed was 76.86m /min, a large number of nanocrystals were found in the high-power scanning image at the top of the cladding layer, and the size was smaller, about 20-100nm, as shown in Fig. 9 (d). It indicates that the formation of nanocrystals is related to the scanning speed of laser cladding, and the higher the scanning speed is, the easier it is to form.
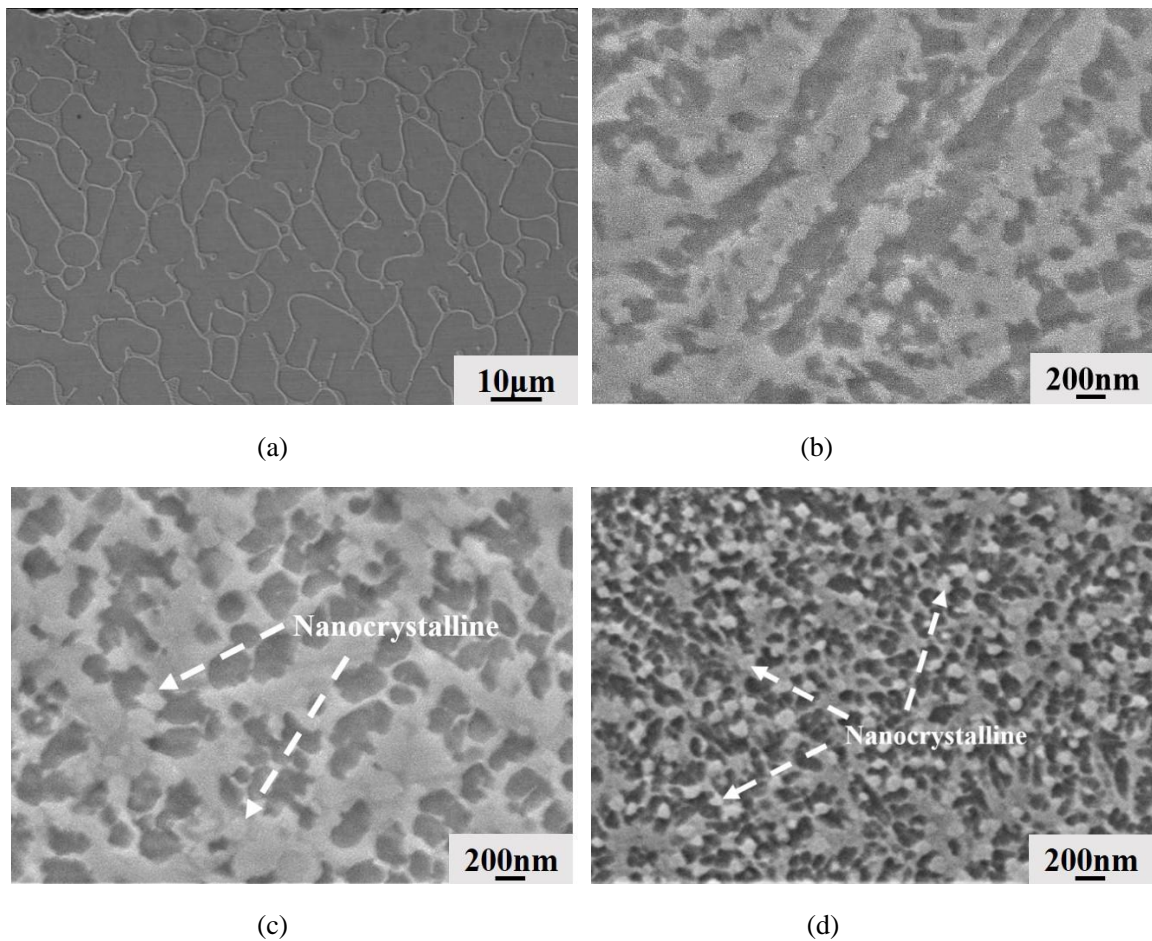

Fig. 9 Microstructure near the top surface at different laser scanning speed: (a) 0.6 m/min, (b) 37.68 m/min, (c) 58.02 m/min, (d) 76.86 m/min

3.3 Cooling rates

To analyze the microstructure characteristics of each area of traditional laser cladding and high-speed laser cladding coating, as well as the influence of different cladding speeds on the

cooling rate, the spacing of secondary dendrite arms in the bottom region, the middle region and the top region of cladding coating were measured by ImageJ software respectively. The relationship between the distance between the secondary dendrite arms and the cooling rate T follows the formula (2) [21].

$$\lambda_2 = A(G \times R)^{-n} \qquad (2)$$

In this equation, A and n are the material constants, G is the temperature gradient and R is the growth rate, and G×R is the cooling rate. The equation shows that the spacing of secondary dendrite arms is inversely proportional to the solidification rate and temperature gradient. Since the temperature gradient during laser cladding is very high (about 106 K/mm), the final microstructure will be very fine or very small. Snopiński et al. [22] calculated the constants A and n of laser cladding nickel-based coatings. Formula (3) is the relationship between the secondary arm spacing and the cooling rate of the nickel-based coating.

$$\lambda_2 = 10(G \times R)^{-1/3} \qquad (3)$$

To calculate the cooling rates near the interface, the intermediate region, and the coating surface, the secondary dendrite arm spacing was measured at least 30 times in each region, and its average value was used for calculation. Fig. 10 shows the cooling rate diagram calculated based on the spacing of secondary dendrite arms at the near interface, middle region and top region of the coating. The Y-axis on the left represented the secondary dendrite arm spacing during high-speed laser cladding, and it can be found that the spacing was basically less than 1 μm, while the Y-axis on the right represented the secondary dendrite arm spacing during traditional laser cladding, which varied between 3.9~5 μm. The results show that the secondary dendrite arm spacing decreased by increasing the distance from the interface during high-speed laser cladding, the reason is that the cooling rate varied in

different regions, so the cooling rate from the interface to the surface increased. Based on the theory, G (surface) < G (interface) and R (interface) ≪ R (surface), it can be concluded that (G×R) (interface) < (G×R) (surface). Thus, the cooling rate at the top of the coating was greater than that of the cooling rate near the interface, and the distance between the secondary dendrite arms decreased from near the interface to the top of the coating. When the cladding speed was 76.86m/min, no obvious secondary dendrite arm was formed at the top of the coating, as shown in Fig. 9 (d). The reason is that there were convection, heat transfer and radiation flux between the substrate and the substrate, so the cooling rate increased and the equiaxial dendrite did not have enough time to form a secondary dendrite arm to solidify. In addition, due to the surface tension and high heat transfer, the edge of the cladding layer had a higher solidification rate, and the solidification direction of the microstructure changed [23, 24]. In traditional laser cladding, the spacing of the secondary dendrite arms in each area of the cladding layer was much larger than that of the secondary dendrite arms during high-speed laser cladding. It can be seen from Fig. 7 (a), Fig. 8 (a), Fig. 9 (a) and Fig. 10 that with the increase of the distance between the secondary dendrite and the interface, the dendrite arm spacing first decreased and then increased, which was different from that of high-speed laser cladding. The reason why there was a difference on the top of the coating is that in the traditional laser cladding, when the dendrite grew to the top, although the solidification process of the molten pool was coming to an end, the small temperature gradient in the liquid phase, easy to produce fine dendrite. However, more nucleation particles were also generated in the liquid metal. These particles were not subject to any restriction, and the growth direction was disorderly, showing the characteristics of uneven growth, forming slightly larger dendrites on the top of the coating, which may make the top of the secondary

dendrite arm spacing become larger. According to Formula (2), the cooling rate of each area of the cladding coating at each scanning speed can be calculated, as shown in Fig. 11.
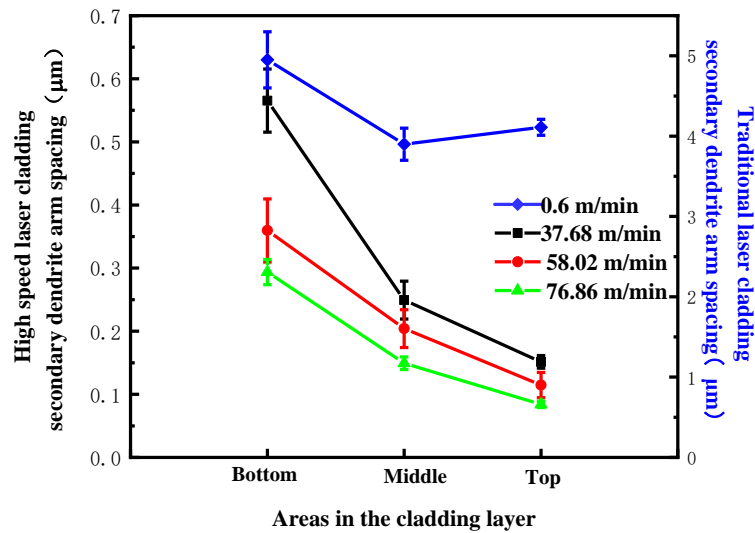

Fig. 10 The distance between secondary dendrite arms in each area of high-speed laser cladding at different scanning speeds
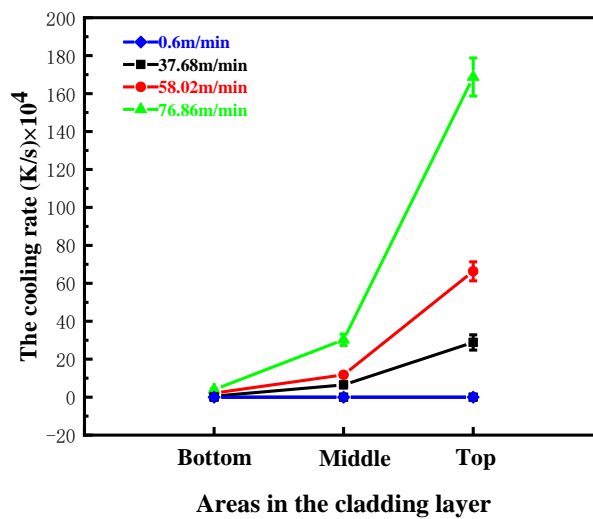

Fig. 11 The cooling rate of each area of high-speed laser cladding at different scanning speeds

As mentioned above, G (surface) < G (interface), R (surface) ≫ R (interface), so (G×R) (surface) > (G×R) (interface). As a result, the cooling rate at the top of the coating was greater than the cooling rate near the interface, and the spacing between the secondary dendrite arms gradually decreased from near the interface to the top of the coating. It can be seen that in traditional laser cladding, when the cladding speed was 0.6m/min, the cooling rate was very

low, and the changes in the three areas were not large. This is because the cladding speed was low at this time, and the G was small. Compared with high-speed laser cladding, the cladding speed was lower, so the residence time in the molten pool was longer than that of high-speed laser cladding, making the cooling time of the molten pool was long and the cooling rate was lower. In addition, with the increase of R and the decrease of G, the laser scanning rate increased from 37.68m/min to 76.86m/min in all three areas of high-speed laser cladding, the cooling rate increased and the secondary dendrite arm spacing decreased. When the scanning rate was 76.86m/min, the cooling rate of the top of the cladding layer reached the maximum value, which was 1.68×10^6 K/s. With the increase of laser scanning rate, R increases and G decreases. This is because the reaction time between the laser and the material was shortened, so the temperature gradient decreased. Since the change of R was more significant than that of G, the value of G×R, representing the cooling rate increased. As a result, the nucleated grains did not have enough time to grow up, thus forming a finer microstructure with smaller secondary dendrite arm spacing, which also indicated that the influence of R on cooling rate was greater than that of G. In addition, when the cooling rate increased, the propulsive rate and thermal gradient of the solid-liquid interface were increased, thereby suppressing the overcooling of the composition of the liquid alloy in the molten pool. Nucleation and growth occurred in more areas of the molten pool, and the microstructure was refined and uniformly distributed [25].

3.4 Phase constitution

The characteristics of laser cladding are rapid heating and rapid cooling, which is a kind of non-equilibrium solidification, which will inevitably lead to supersaturated solid solution and phase lattice distortion in the solidified structure. Due to the great difference between

traditional laser cladding and high-speed laser cladding in the cladding speed, the cooling rate is also considerably different, which may affect the phase composition of the cladding coating. To study the phase difference between the traditional and high-speed laser cladding coating, an X-ray diffractometer was used to determine the phase in the traditional and high-speed laser cladding coating. The diffraction pattern is shown in Fig. 12. The traditional laser cladding sample had a cladding speed of 0.6 m/min, while the high-speed laser cladding test had a cladding speed of 76.86 m/min. It can be seen from Fig. 12 that the phases in traditional laser cladding mainly consist of γ-Ni solid solution、$Cr_{23}C_6$ and Cr_7C_3 type carbides、Cr_2B type chromium boride and $FeNi_3$[26]. While in the high-speed laser cladding, in addition to preserving the original diffraction peaks, a new diffraction peak appeared in the pattern at a diffraction angle of 65°, which was determined by contrast standard diffraction cards as (Fe,Ni) and FeNi phases. By observing Fig. 12 (b), we can find that the spectrum of the traditional laser cladding powder and high-speed laser cladding powder used shows a significantly broadened diffuse peak at about 44°, and there were some weak crystal peaks embedded in it, indicating that the alloy powder used for cladding is mainly amorphous and contains very few crystal phases. Fig. 12 (b) shows that the two alloy powders mainly contain Ni, Fe, Cr and C phases. In addition, using JADE software to retrieve phase and PDF card comparison, it was found that the high-speed laser cladding powder had Fe phase and (Fe, Ni) phase at about 65°, while traditional laser cladding powder did not. Since there was no diffraction peak at 65°, the two phases were not added. However, this also corresponded to the Fig.12 (a), where the diffraction peak appears at about 65° and contains (Fe, Ni) phase.
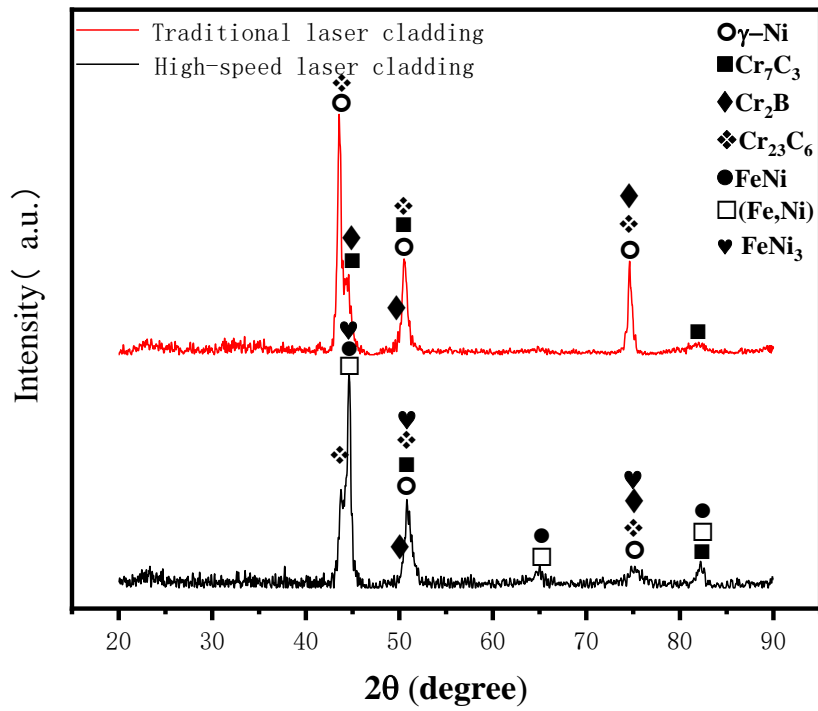
(a) X-ray diffraction patterns of cladding layers
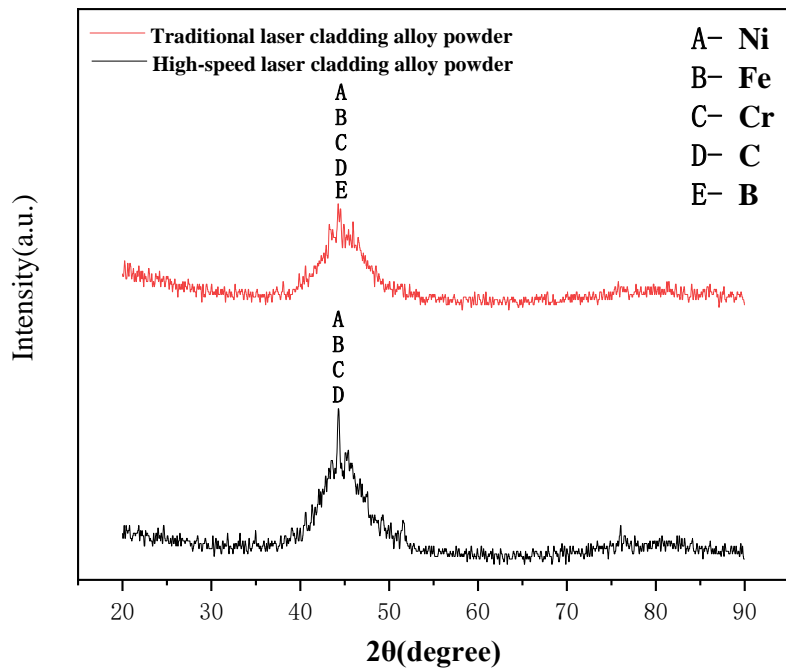
(b) X-ray diffraction patterns of two kinds of alloy powders

Fig. 12 X-ray diffraction patterns of cladding layers and alloy powders

3.5 Coating properties

3.5.1 Microhardness

Fig. 13 shows the surface hardness distribution of traditional and high-speed laser cladding coating. The average microhardness of the surface of traditional laser cladding of Ni45 coating was only 337 $HV_{0.2}$, while the microhardness of the surface of high-speed laser cladding was much higher than that of the traditional laser cladding, all above 500 $HV_{0.2}$. In addition, with the increase of high-speed laser cladding speed, the surface hardness of the coating increased as well. The surface hardness of the coating under three cladding speeds was 503 $HV_{0.2}$, 534 $HV_{0.2}$ and 543 $HV_{0.2}$, respectively increased by 49%, 58% and 61%. Masanta et al. [27] found that the formation of fine tissues at higher cooling rates resulted in an increase in cladding hardness. The microstructure of coating is uniform and fine at the fast cooling rate of high-speed laser cladding, which improves the microhardness of the cladding layer.
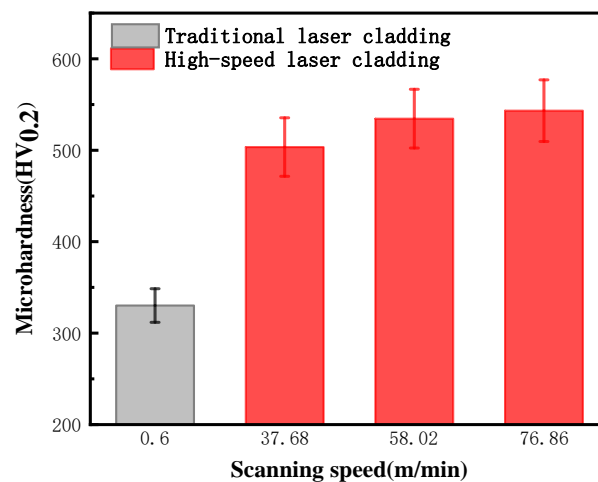

Fig. 13 Surface hardness of laser cladding at different scanning speeds

Fig. 14 shows the microhardness distribution of the cross-section of the traditional and high-speed laser cladding. The microhardness layer was divided into three regions: coating, heat-affected zone and substrate. In traditional laser cladding, the microhardness of the cladding layer was relatively stable, ranging from 330 $HV_{0.2}$ to 340 $HV_{0.2}$, and the

microhardness of the heat-affected zone is 300 $HV_{0.2}$. While in high-speed laser cladding, the microhardness gradually decreased from the coating surface to the substrate direction. From the surface to the bottom, microhardness decreased from about 550 $HV_{0.2}$ to about 450 $HV_{0.2}$. From the microstructure of the high-speed laser cladding, it can be observed that the microstructure characteristics of the top, middle and bottom three regions were also quite different. Transition from the columnar crystal at the bottom to the fine dendritic crystal at the top, the microstructure was gradually refined, and higher microhardness was obtained at the top. This also explains why the hardness of the high-speed laser cladding surface was slightly lower than the top region of the section hardness is that the surface of the cut sample was preground and polished to a certain extent when the surface hardness was tested, so that the hardness tested was slightly lower than the top region of the section. The microhardness of the heat-affected area of high-speed laser cladding was also marginally lower than that of traditional laser cladding, which was about 275 $HV_{0.2}$, the reason is that the cladding speed was faster during high-speed laser cladding, as well as the laser power was lower, the laser heat had less influence on the sample, and the heat-affected area was narrower. It is also observed in Fig. 14 (b) that the overall microhardness of the cladding layer increased with the increase of the cladding speed from 37.68 m/min to 76.86 m/min.
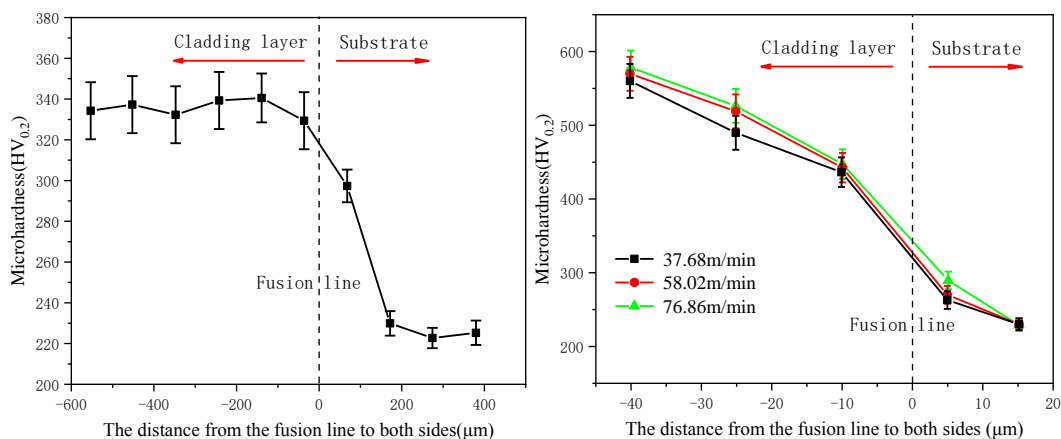
(a) Traditional laser cladding   (b) High-speed laser cladding

Fig. 14 Cross-section hardness values of traditional and high-speed laser cladding coatings

3.5.2 Tribological properties

Under the condition of certain experimental parameters, friction and wear tests were carried out on traditional laser cladding and three sets of high-speed laser cladding coatings with different cladding speeds. The corresponding relationship between friction coefficient and time was compared between traditional laser cladding and high-speed laser cladding with different cladding speeds. The curve of the friction coefficient changing with time is shown in Fig. 15. With the change of time, the friction coefficient also jittered up and down, and the friction coefficient of cladding layer was different at different cladding speeds. In the process of traditional laser cladding friction, the friction coefficient rose steeply and slowly from the initial stage to about 0.63, and then dropped abruptly to about 0.6. Within 0-5 min, it was the initial stage of wear, also known as run-in abrasion. After 5-25 min, the friction coefficient slowly rose to about 0.75 without great fluctuation called the stable wear stage. In high-speed laser cladding, when the cladding speed was 37.68m/min, the friction coefficient rose from the beginning to about 0.6 and then fluctuated up and down periodically. The friction coefficient was similar to the sine function jumping up and down until the end. When the cladding speed was 58.02m/min, the friction coefficient rose to about 0.55 and remained stable, and fluctuated in a small range until the end after 15 min. When the cladding speed was 76.86m/min, the friction coefficient rose rapidly to 0.5 and then remained stable without great fluctuation until the end. The friction coefficient of the traditional laser cladding coating was 0.68, and the friction coefficients of the three groups of high-speed laser cladding coating were lower than that of the traditional laser cladding coating, which was 0.61, 0.57 and 0.52 respectively, indicating that the wear resistance of high-speed laser cladding coating was

better than that of the traditional laser cladding coating. And in the high-speed laser cladding friction and wear test, it can be seen that as the cladding speed increased, the abrasion resistance of the cladding coating also gradually improved. The reason for this phenomenon is that of cladding speed at the same time its microstructure refining, bulky columnar crystals into small dendrites, in larger the cladding coating hardness increased at the same time, the wear resistance of the cladding coating also improved.
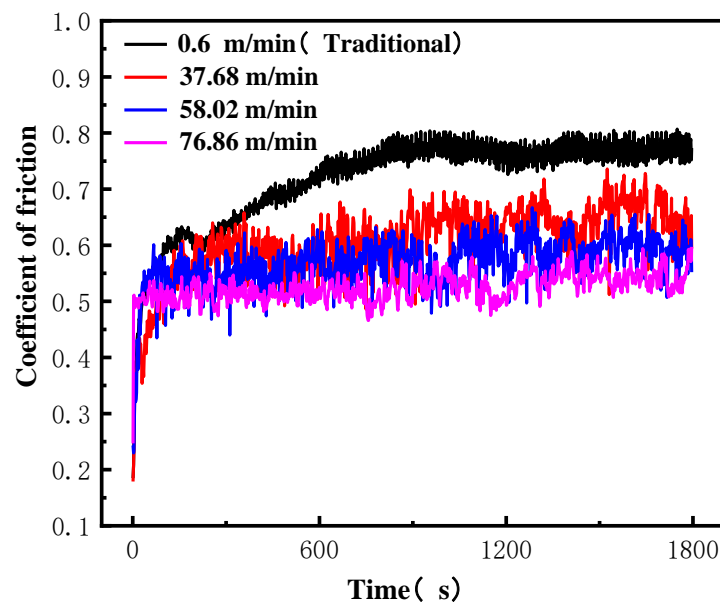

Fig. 15 Variation curve of friction coefficient of laser cladding coating with different scanning speeds over time

Fig. 16 shows the scanning morphology of traditional and high-speed laser cladding after friction and wear under varying parameters. It can be seen that there were many grooves of different depths and wear and tear on the worn-out surface. As for the traditional laser cladding coating, due to the low hardness of the coating, when the friction pair composed of Si_3N_4 ceramic ball was rubbed against each other, the softer part of the cladding coating would be first worn off, then the harder phase would be exposed on the surface layer of the cladding layer, and the wear would be carried out between the ceramic ball and the bump.

Friction and wear process continued, the softer part of the coating surface of the cladding layer was gradually worn off, hard phase and coating bonding strength decreased, and friction was easy to make hard phase fall off from the coating, leaving visible peeling pits on the surface of the coating. In addition, there was also a small amount of abrasive debris on the worn-out surface, indicating that in addition to abrasive wear, adhesive wear has also occurred during the wear process. In the wear process of high-speed laser cladding coating, when the cladding speed was 37.68 m/min, the furrow depth of surface friction of the coating has decreased, and the peeling pits on the surface have also been reduced a lot. When cladding speed was 58.02 m/min, the abrasion of cladding coating has greatly changed, there would be no large ares of exfoliated pits in the wear morphology. From the previous wear resistance analysis, it can be seen that the microstructure of the cladding was more uniform and fine at this time, which improved the mechanical properties of the coating, effectively reduced the wear cutting when rubbing with the Si_3N_4 ceramic ball, and made the surface of wear furrows narrow and shallow, no longer wide and deep, and the number of spalling pits was also greatly reduced. When the cladding speed was 76.86m/min, the furrows worn by the cladding coating became shallower, and there was no obvious wear and peeling. Only the extrusion marks left by the friction with the Si_3N_4 ceramic ball indicated that the coating had better wear resistance. Based on the surface scanning analysis of friction and wear, the traditional laser cladding coating had the most serious spalling and poor wear resistance. The wear and peeling of high-speed laser cladding was improved and its wear resistance was obviously better than that of traditional laser cladding. Furthermore, with the increase of the cladding speed, the friction and wear situation improved in the high-speed laser cladding. When the cladding speed was 76.86 m/min, no obvious peeling pits were found, and the macroscopic wear furrows became

narrow and shallow. In addition, the wear surface of the coating was smooth and some pits and furrows were observed due to the alternating stress of the friction pair. In the study of Kalyanasundaram et al. [28], they electro-deposited nano-diamond particles on aluminum alloy A319, and after using nanoindentation, friction and wear tests, they found that when the microhardness increased, the friction coefficient of the coated sample decreased from 0.60 to 0.32. The experience proved that the microhardness of the coating is the main factor in reducing the wear rate. The hardness increases and the wear resistance of the coating is also enhanced.
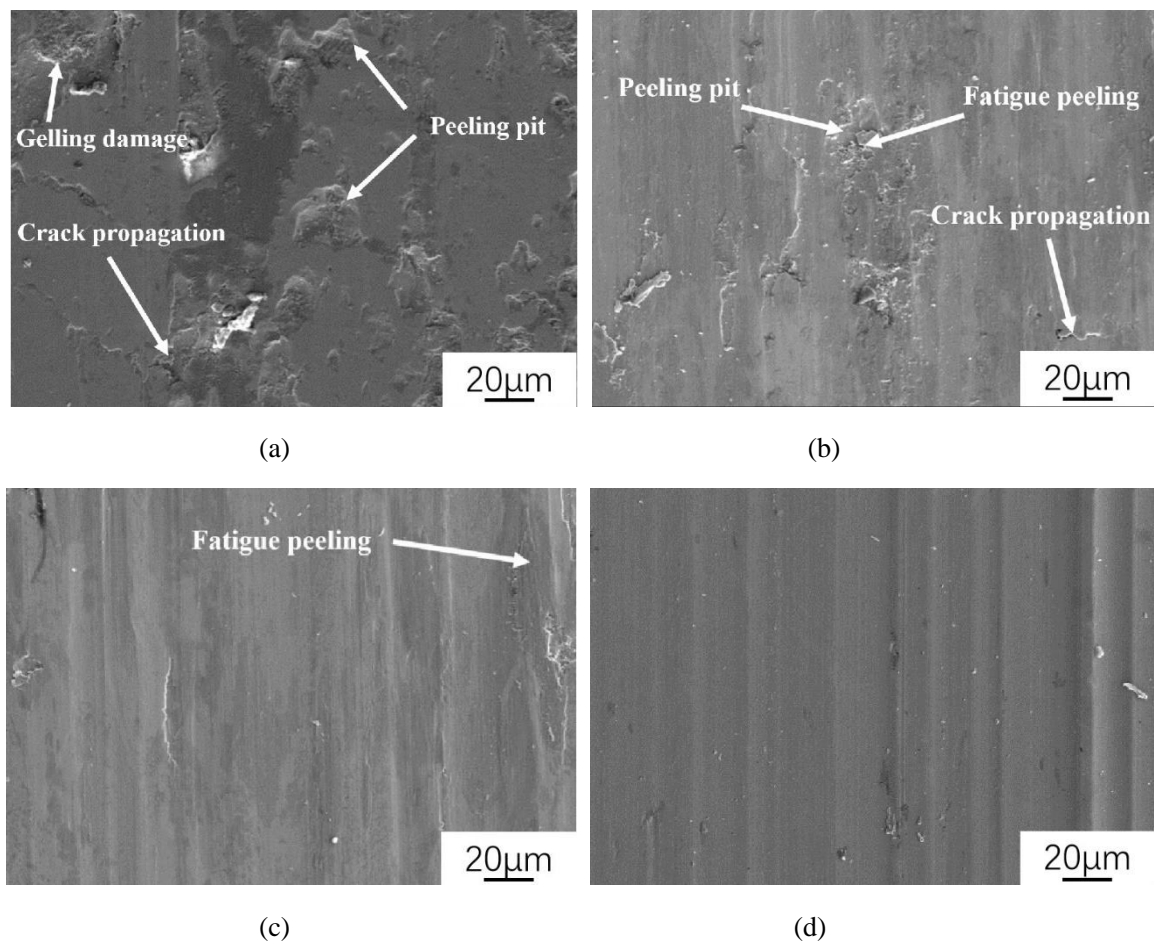

Fig. 16 Morphology of traditional and high-speed laser cladding friction marks: (a) 0.6 m/min, (b) 37.68 m/min, (c) 58.02 m/min, (d) 76.86 m/min

3.5.3 Electrochemical corrosion

Fig. 17 shows the polarization curve of Ni45 cladding coating in 3.5wt% NaCl solution at different cladding speeds. The scan rate was 1 mV/s, and the sample with the laser scan speed of 0.6 m/min was traditional laser cladding, the other three were high-speed laser cladding. It can be seen from Fig. 17 that each polarization curve had roughly the same trend and anodic passivation occurred, but the potential range of the passivation film was slightly different. When the electrode was scanned towards the square sample to a certain potential in the passivation area, the passivation film on the material surface began to dissolve locally under the action of Cl$^-$, and then gradually generated new passivation membrane. When the dissolution rate was greater than its generation rate, pitting pits would occur locally, and the current density would increase rapidly at this time. The corresponding potential was called the breakdown potential (Eb). However, the breakdown potential is easily affected by the self-corrosion potential. It is inaccurate to use the breakdown potential to measure the corrosion resistance of the material. The self-corrosion potential is only a concept of the thermodynamics, and the dynamic characteristics of the material can't be neglected. When evaluating the capability, the corrosion current should be considered first. The corrosion current of the material depends on the dissolution rate of the material. The smaller the corrosion current, the stronger the corrosion resistance of the cladding layer [29].
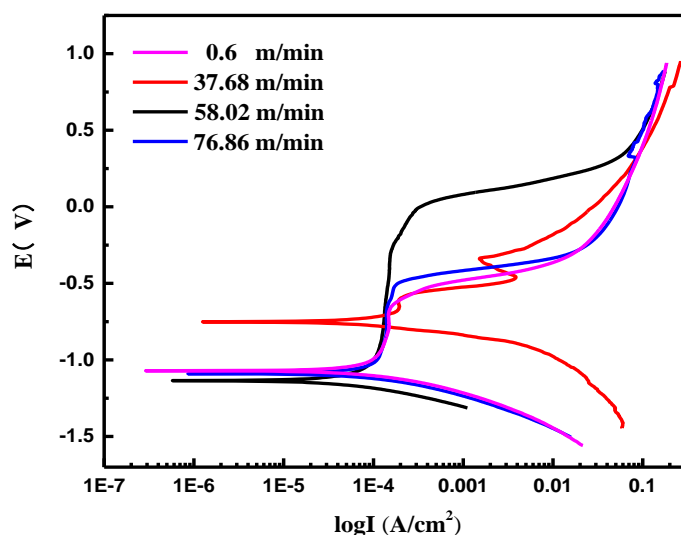
Fig. 17 Electrochemical corrosion polarization curve of the cladding layer at the same cladding speed

　　Using the CView software to fit the obtained polarization curve, the corresponding corrosion current value can be obtained, as shown in Table 5. By comparing the coating polarization curve parameters of the four groups in the table with different cladding speeds, it is found that when the cladding speed was 0.6 m/min, which was the electrochemical test result of traditional laser cladding, the corrosion current density was 1.52E-04 (A/cm^2), larger than the corrosion current of three groups of high-speed laser cladding. For traditional and high-speed laser cladding, the corrosion voltage Ecorr has little changed. It is also observed that the corrosion rates of the three groups of laser cladding samples were lower and the corrosion current density decreases with the increase of the cladding speed. The self-corrosion current density was a symbol of the degree of corrosion of materials. The higher the self-corrosion current density was, the deeper the degree of corrosion of materials would be, indicating that with the increase of the cladding speed in high-speed laser cladding, the corrosion resistance of cladding coating would also be enhanced. When the cladding speed was 76.86 m/min, the electrochemical test results show that the self-corrosion current density and corrosion rate of the cladding layer under this parameter were the lowest. By analyzing the microstructure and phase of the high-speed laser cladding coating, it is found that with the

increase of the cladding speed, the microstructure of the cladding coating was uniform and fine, which was conducive to improving the corrosion resistance of the cladding layer. The existence of nanocrystals was observed on the surface layer of the laser cladding layer with a laser cladding speed of 76.86 m/min. Nanocrystals, on the other hand, can improve the diffusion rate of elements so that a thicker SiO_2 surface film can be formed on the surface, effectively inhibiting the corrosion process of metals [30].

Table 5 Polarization curve parameters of cladding layers at different cladding speeds

Cladding speed （m/min）	Corrosion current density (A/cm^2)	Self-corrosion potential (V)	Corrosion rate CR (mm/a)
0.6	1.52E-04	-1.0703	3.35818
37.68	1.17E-04	-0.7511	2.7543
58.02	8.73E-05	-1.035	2.0586
76.86	1.12E-05	-1.0808	0.26434

4 Conclusions

(1) Compared with traditional laser cladding, high-speed laser cladding coating had low roughness and thinner coating. At a high laser cladding rate, the R value (growth rate of dendritic crystal tip) increased, leading to a decrease in the G/R ratio (tissue supercooling), and the microstructure tended to be equiaxial dendritic structure. Therefore, as the scanning rate increased from 37.68 m/min to 76.86 m/min, the microstructure of the coating gradually refined, and nanocrystals with a size of 20-100 nm were observed in the top region when the cladding rate was 76.86 m/min.

(2) The coating cooling rate increased with the increase of cladding speed in high-speed laser cladding. When the cladding speed increased from 37.68 m/min to 76.86 m/min, the secondary dendrite arm in each area of the cladding coating decreased and its cooling

rate increased. The spacing between the secondary dendrite arms from the interface region to the top region decreased gradually. When the cladding speed was 76.86 m/min, the top cooling rate was 100 times higher than the bottom cooling rate. In contrast, the cooling rates of each area of traditional laser cladding did not vary much.

(3) The microhardness of the cross-section of the traditional laser cladding coating was relatively uniform, and the top of the coating was not much different from the interface area, while the top hardness of the high-speed laser cladding coating > the middle hardness > the bottom area hardness. The reason for this is that the regional cooling rate of large difference in microstructure size was large, and in addition, nanocrystals were generated at the top area at a very high cooling rate, which greatly enhanced the microhardness.

(4) With the increase of laser cladding speed, the microstructure was refined continuously, and the coarse columnar crystals were transformed into fine dendrites. While the hardness of the cladding coating was greatly improved, the wear resistance of the cladding coating also improved.

(5) The corrosion resistance of the high-speed laser cladding coating was better than that of traditional laser cladding, and the presence of nanocrystals in the surface layer of the cladding layer with a laser cladding speed of 76.86 m/min improved the element diffusion rate, which enabled the surface to generate thicker SiO_2 surface film, effectively inhibiting the corrosion process of metal and enhancing the corrosion resistance of the coating.

Acknowledgements

References

[1] Anonymous, Analyzing Wear and Tear of Metal, (2020).

[2] M. Sigvant, M. Sigvant, J. Pilthammar, J. Hol, J.H. Wiebenga, T. Chezan, B. Carleer, A.H. van den Boogaard, Friction and lubrication modelling in sheet metal forming simulations of the Volvo XC90 inner door, Journal of Physics: Conference Series, 734 (2016) 032090 (4pp).

[3] D. Tromans, Elastic Anisotropy of HCP Metal Crystals and Polycrystals, (2011).

[4] A.M. M., B.D.R. M., T.A.M. D., P. C., J. L., J.S. D., The effect of hard chrome plating on iron fines formation, TRIBOL INT, 142 (2020).

[5] M.G. Nicole, A.K. Michael, H.M. Diem, S. Mina, M.P. Deborah, Occupational exposure to hexavalent chromium and cancers of the gastrointestinal tract: A meta-analysis, CANCER EPIDEMIOL, 34 (2010).

[6] A. A., C. F., G.D.B. J., C.D.H. J., M. R., S. A., U. S., V. P., HVOF-Deposited WCCoCr as Replacement for Hard Cr in Landing Gear Actuators, J THERM SPRAY TECHN, 20 (2011).

[7] K. Jarkko, P. Jouni, H. Esa, K. Heli, V. Petri, Characterization of Powder-Precursor HVOF-Sprayed Al 2 O 3 -YSZ/ZrO 2 Coatings, J THERM SPRAY TECHN, 28 (2019).

[8] X. Haiyan, L. Tao, L. Haibo, W. Xinlin, Z. Hongchao. Study on quality prediction and path selection of 316L laser cladding. Laser Technology, 42 (2018) 53-59.

[9] X. Wenchao, S. Boxue, Z. Yu, Y. Tianbiao, W. Jun, Geometry and dilution rate analysis and prediction of laser cladding, The International Journal of Advanced Manufacturing Technology, 103 (2019).

[10] T. Schopphoven, A. Gasser, G. Backes, EHLA: Extreme High-Speed Laser Material Deposition, Laser Technik Journal, (2017) 45-45.

[11] K.G. Damian, R. Agnieszka, A.D. Stanis, M. Jerzy, M. Ukasz, K. Axel, Improvement of Corrosion Resistance of 13CrMo4-5 Steel by Ni-Based Laser Cladding Coatings, J MATER ENG PERFORM, (2020).

[12] L. Lou, Y. Zhang, Y. Jia, Y. Li, H. Tian, Y. Cai, C. Li, High speed laser cladded Ti-Cu-NiCoCrAlTaY burn resistant coating and its oxidation behavior, SURF COAT TECH, 392 (2020).

[13] N.S. N, V.M. A, Y.M. I, NiCrBSi coating obtained by laser cladding and subsequent deformation processing, Journal of Physics: Conference Series, 946 (2018).

[14] X. Qing-Long, Z. Yu, L. Sen-Hui, L. Chang-Jiu, L. Cheng-Xin, High-temperature oxidation behavior of CuAlNiCrFe high-entropy alloy bond coats deposited using high-speed laser cladding process, SURF COAT TECH, 398 (2020).

[15] D. Moore, Protective finishing systems for navy aircraft, ADV MATER PROCESS, 155 (1999) 31-34.

[16] L. Weiping, N.D. J., Fabrication of functionally graded TiC/Ti composites by Laser Engineered Net Shaping, SCRIPTA MATER, 48 (2003).

[17] Z. Jian, X. Dezhen, C. Xiaoying, D. Xiangdong, R. Xiaobing, S. Jun, Dislocation induced strain glass in Ti 50 Ni 45 Fe 5 alloy, ACTA MATER, 120 (2016).

[18] P. Yichao, Z. Maicang, D. Chenyang, D. Xinjian. High temperature vacuum carburization behaviors and phase evolution mechanisms of Cr35Ni45Nb alloy under service condition. Acta Metallurgica Sinica Chinese Edition, 51 (2015) 11-20.

[19] D. Zhenjing, Y. Qingan, L. Changhe, D. Lan, B. Xiufang, Z. Yanbin, Y. Min, J. Dongzhou, L. Runze, L. Zhanqiang, Milling force and surface morphology of 45 steel under different Al 2 O 3 nanofluid concentrations, The International Journal of Advanced Manufacturing Technology, (2020).

[20] K. Laurens, Principles of Solidification, MATER TODAY, 14 (2011).

[21] A.K. G., J.C. M., J.H. T., D.R. A., F.H. W., INCONEL 718: A solidification diagram, Metallurgical Transactions A, 20 (1989).

[22] A.S. Przemys, K. Mariusz, T. Tomasz, K. Beata, Effect of cooling rate on microstructural development in alloy ALMG9, J THERM ANAL CALORIM, 133 (2018).

[23] A. T., F. H., The effect of cooling rate on the solidification of INCONEL 718, Metallurgical and Materials Transactions B, 36 (2005).

[24] M.S. Raghvendra, E. Jürgen, L.S. Wolfgang, K.D. Brij, S. Ludwig, Cooling Rate Evaluation for Bulk Amorphous Alloys from Eutectic Microstructures in Casting Processes, MATER TRANS, 43 (2002).

[25] V. Thiévenaz, T. Séon, C. Josserand, Solidification dynamics of an impacted drop, J FLUID MECH, 874 (2019) 756-773.

[26] Z. YM, L. XG, Z. W, L. GY, Synthesis of FeNi3/(Ni0.5Zn0.5)Fe2O4 nanocomposite and its high frequency complex permeability, NANOTECHNOLOGY, 18 (2007) 15701-1-15701-5-0.

[27] S.M. Shariff, A. Roy Choudhury, M. Masanta, Evaluation of modulus of elasticity, nano-hardness and fracture toughness of TiB_2-TiC-Al_2O_3 composite coating developed by SHS and laser cladding, Materials Science & Engineering, A. Structural Materials: Properties, Misrostructure and Processing, 528 (2011) 5327-5335.

[28] K. D., M. P., Electrodeposition of nanodiamond particles on aluminium alloy A319 for improved tribological properties, MICRO NANO LETT, 3 (2008) 110-116.

[29] L. Long-yuan, Book review: Corrosion of Steel in Concrete-Prevention, Diagnosis, Repair, MAG CONCRETE RES, 67 (2015).

[30] E. M., S.H. M., K. S., M.E. E., S. M., C. R., Some surfactants in the series of 2-(alkyldimethylammonio) alkanol bromides as inhibitors of the corrosion of iron in acid chloride solution, CORROS SCI, 37 (1995).